Removal of water-soluble inorganic arsenicals with phosphorene oxide nanoadsorbents: A first-principles study

Kerry Wrighton-Araneda[1], *Diego Cortés-Arriagada*[1,*]

[1]Programa Institucional de Fomento a la Investigación, Desarrollo e Innovación. Universidad Tecnológica Metropolitana. Ignacio Valdivieso, 2409, P.O. Box 8940577, San Joaquín, Santiago, Chile. *Corresponding author: E-mail address: dcortes@utem.cl

Abstract: A complete picture of the phosphorene oxide (PhosO) sorption properties for the simultaneous removal of inorganic As(III) and As(V) pollutants from water has been developed using first-principles calculations. Calculated adsorption energies, competitive adsorption with co-existing species, energy decomposition analyses (ALMO-EDA), implicitly/explicitly solvated geometries, and adsorption free energies provide deep insights into the adsorption mechanism as well as the origin of the strong selectivity sorption ability. The PhosO nanoadsorbents establish inner-sphere surface complexes with arsenicals even under competition with water molecules. These proposed structures also show a strong affinity with the highly mobile As(III), where energy saving is achieved by avoiding the pre-oxidation process to convert As(III) into As(V) as requested in related materials. Results show that electrostatic driving forces govern the adsorption of neutral arsenicals, while the interplay between electrostatic and polarization phenomena drives the uptake of anionic arsenicals. By computing the adsorption strength as a function of the oxidation degree, the optimum adsorption efficiency is reached with a 25% in the content of oxidizing groups. In this oxidation degree, the strong repulsive surface charge at high pH turns the PhosO nanoadsorbents convenient to recycle via simple treatment with alkaline eluents. Finally, the adsorption ability remains thermodynamically allowed in a wide range of ambient temperatures (enthalpically governed reaction). Conceptually understanding the sorption properties of phosphorene-oxide-based materials towards arsenic pollutants provides a useful framework for future water treatment technologies.

Keywords: Phosphorene; nanotechnology; surface science; nanomaterials; environmental chemical engineering.

1. Introduction

Arsenicals are highly toxic compounds whose chronic exposure has been associated with carcinogenic, endocrine, cardiovascular diseases, skin and lung damage, diabetes, and metabolic syndrome[1–4]. The arsenic toxicity is related to its ability to replace phosphate groups in biomolecules, showing a strong affinity with –SH groups of cysteinyl residues[5,6]. Among the removal/remediation strategies, adsorption is eco-friendly, economical, efficient, and simple. The solid-phase adsorption reduces undesirable by-products, adsorbent materials separate by filtration and recovered for repetitive uses applying simple basic/acid treatment[7,8]. In this regard, novel layered materials for arsenic sorption have emerged as new alternatives to commercial adsorbents, featuring a large surface area, high adsorption capacity, straight synthesis, and easy recovery. Graphene oxide composites (with chitosan and metal oxides)[9–13] demonstrated efficient arsenic removal from different water sources, where adsorption performance enhances depending on the graphene oxidation degree[14]. The arsenic adsorption capacity of graphene oxide also increases by inner-sphere complexation, especially using hydroxyl and carboxyl groups as oxidizing groups[15].

Phosphorene is a layered and puckered hexagonal nanostructure of phosphorous atoms linked by covalent bonds and weak interlayer dispersive interactions[16–18], which shows a lamellar structure, high carrier mobility, high chemical stability, and tunable bandgap (~0.3-2.0 eV)[19–21]. Phosphorene-based nanoadsorbents have been proposed to uptake pollutants such as formaldehyde, nitrogen oxides, and carbon oxides[22,23]. Phosphorene has also been applied for simultaneous As(III)/As(V) removal from water at neutral conditions, showing higher adsorption efficiency than graphene (4.8-20.0 mg/g v. 1.33 mg/g)[24,25]. Thus, phosphorene-based materials appear as new promising candidates

for water treatment by adsorption in the solid-phase, outstripping graphene(oxide)-based materials. Besides, surface oxidation is reported to increase the arsenic adsorption efficiency for layered materials such as graphene oxide[12,14]. In the phosphorene case, synthesis at partially oxidized forms results in highly stable phosphorene oxides[26], which does not alter its two-dimensional (2D) structure. Additionally, different O:P ratios play a key role in the phosphorene properties (chemical stability, band structure, work-function, transport properties, among others)[23,26–31]. First-principles calculations show that the increased oxygen content decreases the phosphorene bandgap in the range of 1.0–1.3 eV[29]. Otherwise, phosphorene oxides obtained from black phosphorene show a straightforward synthesis compared to those based on blue phosphorene, where time demanding methods such as epitaxial growth are employed[26,32]. Therefore, the application of oxidized phosphorene nanoadsorbents based on black phosphorene could be a promising strategy for arsenic removal from polluted waters. However, minor efforts have been developed to characterize such applications to the best of our knowledge.

Herein, we proposed phosphorene-oxide-based nanoadsorbents for the simultaneous removal of highly toxic inorganic As(III) and As(V) species from water. Employing density functional theory (DFT) calculations, it is studied the adsorbent–adsorbate stability, interaction mechanisms, arsenic mobility, and sorbent regeneration. The proposed nanoadsorbents show unique advantages: i) adsorption mechanism *via* inner-sphere surface complexation; ii) strong adsorption efficiency with a medium oxidation degree (oxygen content); iii) high recovery ability by simple treatment methods with alkaline eluents. Then, phosphorene-oxides turn into remarkable candidates for further control and remediation technologies of arsenic contamination from water.

2. Computational Details

Phosphorene nanoadsorbents (**Phos**, $P_{126}H_{30}$) were used for the adsorption studies with a surface area of 1583 $Å^2$ considering its electron density, which are relatively larger to obtain well-converged adsorption energies concerning the arsenic surface (up to ~166 $Å^2$). Phosphorene oxide (**PhosO**) was studied in O:P ratios of 1:8, 1:4, 1:2, and 1:1, whose geometrical structures have been early reported[29]. According to the O:P ratio, the nanoadsorbent models were called **PhosO(1:8)**, **PhosO(1:4)**, **PhosO(1:2)**, and **PhosO(1:1)**. A model containing a single oxygen atom [**PhosO(1:∞)**] was included for comparative purposes. Inorganic arsenicals were considered in As(III) and As(V) oxidation states.

Calculations were performed with the PBE functional and all-electron def2-SVP basis sets functional in the ORCA 4.1 program[33–35]. Dispersion force corrections for self-consistent field energies were included with the DFT-D3 method (with the Becke-Johnson damping function)[36]. The SMD solvation model was used to include solvent effects in water (ε=80.4), which is based on the charge density of a solute molecule interacting with a continuum description of the solvent[37]. Molecular structures were optimized without geometrical constraints; convergence tolerance values of 1×10^{-8} and 1×10^{-6} Ha were used for SCF and geometry optimization steps, respectively. The adsorbent-adsorbate stability was characterized by the adsorption energy (E_{ads}):

$$E_{ads}=E_{na}+E_{ad}-E_{na-ad} \quad (1)$$

where E_{na}, E_{ad}, and E_{na-ad} are the total energies of the free nanoadsorbent, free adsorbate, and the adsorbent-adsorbate system, respectively. Accordingly, the more positive the E_{ads} values, the more stable the adsorbent-adsorbate complex is. E_{ads} values includes the counterpoise

correction avoid basis set superposition errors[38]. Moreover, adsorption energies were further decomposed into physical contributions by the energy decomposition analysis based on absolutely localized molecular orbitals (ALMO-EDA) in the Q-Chem program[39,40]. Accordingly, the adsorption energy for one AB complex is expressed as:

$$-E_{ads} = \Delta E_{CT} + \Delta E_{POL} + \Delta E_{DISP} + \Delta E_{ELEC} + \Delta E_{PREP} + \Delta E_{PAULI} \quad (2)$$

Where ΔE_{CT}, ΔE_{POL}, ΔE_{DISP}, and ΔE_{ELEC} stand for the stabilizing energy due to charge transfer effects (inter and intramolecular charge flow between fragments), polarization effects (induced electrostatic), dispersion forces (van der Waals interactions), and Coulombic attractions (classical intermolecular electrostatic), respectively. ΔE_{PAULI} is the energy destabilization due to steric Pauli repulsion. ΔE_{PREP} is the destabilizing geometric/electronic preparation energy required by fragments to reach the complex geometry.

Global reactivity indexes [chemical potential (μ), molecular hardness (η), and electrophilicity (ω)] were calculated as $\mu = \frac{1}{2}(E_L + E_H)$; $\eta = \frac{1}{2}(E_L - E_H)$; $\omega = \mu^2/2\eta$, where E_L and E_H are the LUMO and HOMO energies, respectively[41]. The chemical signature of intermolecular interactions was analyzed by the Atoms-in-Molecules (AIM) method[42]. In this way, it was obtained the electron density (ρ_i) of the bond critical points (BCPs) connecting fragments through intermolecular bond paths and serves as a measure of the interaction strength. Under this framework, covalent bonds reach ρ_i values of ~0.1–0.5 e/Bohr^3 (and depending on the polar bond character), coordinate and hydrogen bonds (closed-shell interactions) takes values of $\rho_i \approx 0.04–0.10$ e/Bohr^3, and weak electrostatic interactions are characterized by $\rho_i \leq 0.01$ e/Bohr^3. AIM, Mulliken charges, and wavefunction analyses were obtained in the Multiwfn 3.6 code[43].

3. Results and Discussions

3.1. PhosO nanoadsorbents

First, we analyzed some relevant electronic/chemical properties of the **PhosO** nanoadsorbents (Table 1). The HOMO-LUMO energy difference (Δ_{HL}) of intrinsic phosphorene is ~1.3 eV, denoting its semiconducting character in agreement with those reported for cluster models of phosphorene (~1.5 eV)[44]. Phosphorene oxides show Δ_{HL} values in the range of 1.1-1.3 eV, agreeing with those reported by Wang et al. (1.0–1.3 eV)[29]. Thus, the phosphorene oxidation (in O:P ratios from 1:8 to 1:1) almost does not affect the bandgap with respect to intrinsic phosphorene.

Regarding the chemical reactivity, the maximum hardness principle states stable systems are associated with a relatively higher molecular hardness[47]. The **PhosO** nanoadsorbents display a similar molecular hardness compared to intrinsic phosphorene (η=0.6–0.7 eV), denoting that the oxidation almost does not affect the chemical stability of phosphorene. Also, μ is related to the electronegativity χ through $\mu=-\chi$; while ω is the gained stability when the molecular system gains electrons. Hence, μ and ω are related to the relative electrophilic character[41]. Due to the oxidizing groups, the **PhosO** electrophilic character is slightly increased than phosphorene (μ=–4.4 eV; ω=15.2 eV). Note that the molecular

Table 1. Electronic properties of phosphorene (**Phos**) and phosphorene oxides (**PhosO**). μ, η, ω and Δ_{HL} are in eV. μ_D is in Debye.

	Δ_{HL}	η	μ	ω	μ_D
Phos	1.3(1.0-1.6)[29,44,45]	0.6 (0.7)[46]	-4.4(-5.0)[46]	15.2(17.2)[46]	0.1
PhosO(1:∞)	1.3	0.7	-4.4	14.7	5.9
PhosO(1:8)	1.3(1.3) [29]	0.7	-4.5	15.2	31.3
PhosO(1:4)	1.2(0.85-1.3) [29,30]	0.6	-4.6	18.2	60.1
PhosO(1:2)	1.1(1.0) [29]	0.6	-4.8	21.0	60.1
PhosO(1:1)	0.3(0.6) [29]	0.1	-5.5	107.4	48.4

hardness considerably decreases in highly oxidated phosphorene [**PhosO(1:1)**], and the electron acceptor character increases drastically. Thus, highly oxidated phosphorene has high reactivity, turning it chemically unreliable for practical applications. In other words, highly oxidated phosphorenes will be easily converted to lower O:P ratio systems through reduction reactions due to its strong acceptor character.

Otherwise, dipole moments (μ_D) of the **PhosO** structures increase compared to intrinsic phosphorene due to the electronegativity difference between phosphorus and oxygen atoms [P (2.1) and O (3.5), in the Allred-Rochow scale][48]. Consequently, oxygen atoms in **PhosO** are negatively charged (~–0.3|*e*|), while phosphorous atoms show positive charges (~+0.2|*e*|). In this way, surface oxygen atoms turn in adsorption sites, improving either the attack of electrophilic groups or increasing the adsorption efficiency *via* hydrogen bonding. However, a high O:P ratio in **PhosO(1:2)** and **PhosO(1:1)** is expected to cause a strong repulsive surface of negative charge due to the high oxygen content, reducing the adsorption efficiency of anionic adsorbates or adsorbates with nucleophilic groups.

3.2. Arsenic–PhosO interaction

Inorganic arsenicals (arsenite and arsenate) behave as triprotic acids in solution and dissociate in water with different acid-base equilibrium depending on the pH[1,49]:

$$As(OH)_3 \Leftrightarrow H^+ + AsO(OH)_2^- \qquad pKa_1=9.2 \qquad (3)$$

$$AsO(OH)_2^- \Leftrightarrow H^+ + AsO_2(OH)^{2-} \qquad pKa_2=12.1 \qquad (4)$$

$$AsO_2(OH)^{2-} \Leftrightarrow H^+ + AsO_3^{3-} \qquad pKa_3=13.4 \qquad (5)$$

$$AsO(OH)_3 \Leftrightarrow H^+ + AsO_2(OH)_2^- \qquad pKa_1=2.3 \qquad (6)$$

$$AsO_2(OH)_2^- \Leftrightarrow H^+ + AsO_3(OH)^{2-} \qquad pKa_2=6.8 \qquad (7)$$

$$AsO_3(OH)^{2-} \Leftrightarrow H^+ + AsO_4^{3-} \qquad pKa_3=11.6 \qquad (8)$$

Considering removal applications are carried out at almost neutral conditions onto aqueous matrices (pH≈7), As(III) is non-deprotonated at neutral pH; thus, neutral $As(OH)_3$ [henceforth, As(III)] was selected for sorption studies. Conversely, As(V) is neutral only at low pH, but it deprotonates when pH≥2.3; thus, $AsO_2(OH)_2^-$ and $AsO_3(OH)^{2-}$ [henceforth, $As(V)^-$ and $As(V)^{2-}$, respectively] are dominant in the range of removal applications, choosing these structures for sorption studies.

Fig. 1 displays the adsorbent-adsorbate systems. Arsenicals are adsorbed onto intrinsic phosphorene with intermolecular distances of up to 3.0 Å *via* non-covalent bonding, which agrees with previous results[50,51]. In the case of oxidized phosphorene, the arsenic uptake is dominated by intermolecular hydrogen bonding with H···O(**PhosO**) bond lengths in the range of 1.6–2.9 Å, including also long-range intermolecular O···P(**PhosO**) bonding of up to 2.6 Å. Therefore, arsenicals are adsorbed onto **PhosO** nanoadsorbents through inner-sphere surface complexation.

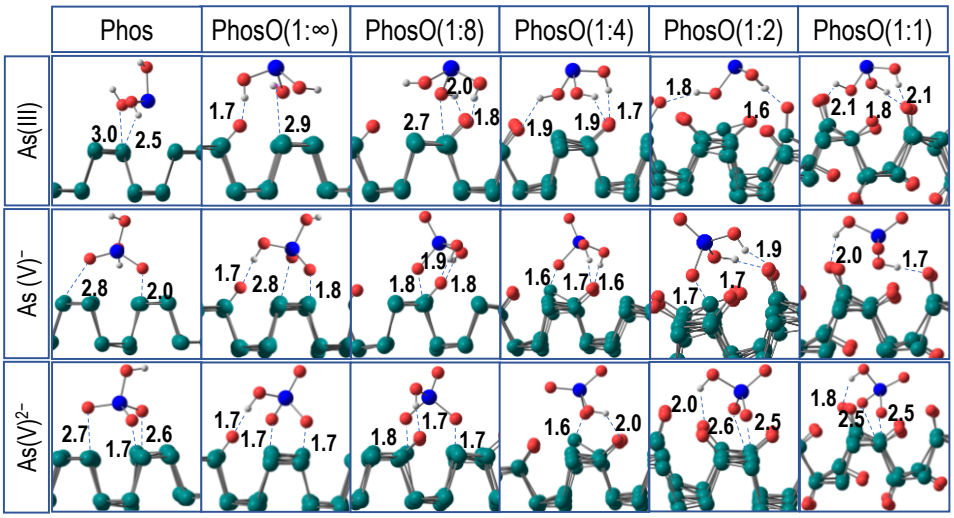

Fig. 1. Molecular structures of arsenicals and their complexes with phosphorene (**Phos**) and phosphorene oxides (**PhosO**). Distances are in Å. Color code: white (H), red (O), green (P), and blue (As).

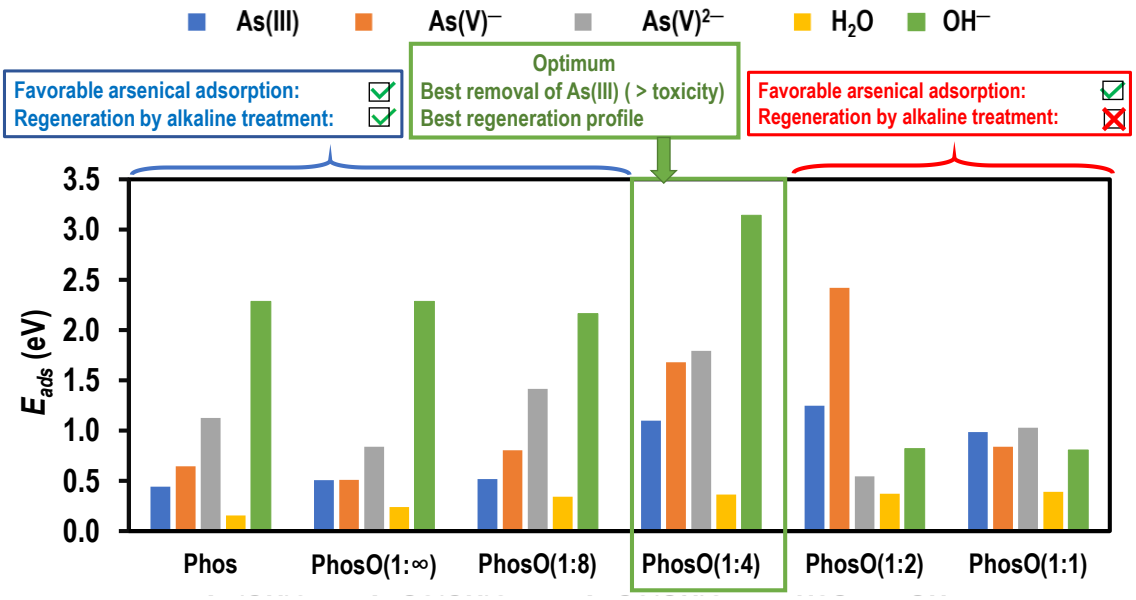

Fig. 2. E_{ads} of water, trivalent, pentavalent arsenicals, and hydroxyl anion adsorbed onto intrinsic phosphorene (**Phos**) and phosphorene oxide (**PhosO**).

Fig. 2 displays the adsorption energies in aqueous solution. For the most part, the adsorption stability increases as the adsorbate negative charge increases, i.e., $E_{ads}[As(III)]<E_{ads}[As(V)^{-}]<E_{ads}[As(V)^{2-}]$. As a reference, the arsenic adsorption onto intrinsic phosphorene is reached with positive adsorption energies of ~0.4, 0.6, and 1.1 eV for As(III), $As(V)^{-}$, and $As(V)^{2-}$, respectively. Then, phosphorene adsorbs arsenicals from aqueous sources with remarkable stability, as noted from previous experimental and theoretical studies[50,51].

Otherwise, the arsenic uptake onto phosphorene oxide is examined according to the oxidation degree. For comparative purposes, the arsenic uptake onto a very low oxidized **PhosO** surface [**PhosO(1:∞)**] slightly increases the E_{ads} values (up to 15%) with respect to the pristine phosphorene. Consequently, intrinsic phosphorene and reduced phosphorene oxides with a very low-oxidized character perform similarly in arsenic removal. Conversely, medium-oxidized **PhosO** nanoadsorbents [**PhosO(1:8)**, **PhosO(1:4)**] considerably improve

the adsorption performance *via* the formation of inner-sphere surface complexes, increasing the E_{ads} values up to 160% with respect to intrinsic phosphorene. As an illustration, As(III), $As(V)^{-}$, and $As(V)^{2-}$ reach E_{ads} values of ~1.1, 1.7, and 1.8 eV onto **PhosO(1:4)**, respectively. Interestingly, the As(III) adsorption strength increases up to ~38% compared to oxidized graphene (E_{ads}≈0.8 eV)[52], which require chemical functionalization with minerals for an efficient arsenic adsorption in composite materials[10,12,13]. Remarkably, related mineral oxides have shown E_{ads} values of ~1.1 eV for As(III) removal (e.g., gibbsite, iron oxides, and titanium dioxides), which have been widely described as efficient arsenic adsorbents[53–57]. Hence, medium-oxidized **PhosO** structures are excellent arsenic nanoadsorbents compared to mineral surfaces, allowing them to reach adsorption energies above 1.1 eV without requiring extra chemical functionalization and reducing the costly and time-consuming methods for the synthesis of composites.

It is also important to highlight that because of the weak affinity towards As(III) of several adsorbents, the arsenic treatment technologies require the pre-oxidation of As(III) to As(V) to allow the efficient uptake. Pre-oxidation is used in technologies employing iron coagulants, nanofiltration by thin-films, and membrane-integrated hybrid systems[58–60]. These processes turn costly and time-consuming due to the operational complexity, make use of strong oxidants (H_2O_2 and $KMnO_4$) or photocatalysts (TiO_2) in the pre-oxidation process. Therefore, medium-oxidized **PhosO** structures could be implemented as excellent nanoadsorbents for simultaneously and directly removal of As(III) and As(V), where energy saving is achieved by avoiding the pre-oxidation process to convert As(III) into As(V).

In contrast, highly oxidized phosphorene [**PhosO(1:2)** and **PhosO(1:1)**] show a not ideal adsorption behavior as a result of the strong negatively charged surface, leading to a strong adsorbent–adsorbate electrostatic repulsion, and consequently, decreasing the adsorption performance. For instance, the adsorption energy of $As(V)^{2-}$ onto **PhosO(1:2)** is decreased with respect to the uptake onto medium-oxidized **PhosO** (0.5 v. 1.8 eV) . Then, a high/full phosphorene oxidation does not provide additional adsorption performance compared to medium-oxidized phosphorene.

3.3. Water competitivity and recovery

We also analyzed the adsorption stability of water molecules (H_2O) and hydroxide anions (OH^-) onto phosphorene oxide (Fig. 2). First, the adsorption energy of the **H_2O–Phos(PhosO)** complexes is always lower (at least 65 %) compared to those reached by complexation of arsenicals, indicating arsenicals are selectivity adsorbed in an aqueous solution. In other words, water molecules are non-competitive factors for arsenic removal with phosphorene oxide-based materials.

Another key feature for any water treatment technology is the use of sorbent materials by several adsorption-desorption cycles. For regeneration and reusability of nanostructured adsorbents, surface treatment with alkaline eluents (e.g., NaOH) allows the sorbent regeneration by removing ~99% of arsenic from graphene-oxide composites with metal oxides such as $CuFe_2O_4$, Gd_2O_3, Fe_3O_4, and CuO), Zn-Fe mixed metal oxides, Fe_3O_4/Halloysite nanocomposites, Fe/Cu-polyurethane nanoparticles, and Ti-oxides[13,55,61,62]. Therefore, the phosphorene oxide reusability as a function of the oxidation degree was investigated by considering hydroxide (OH^-) anions as eluents.

Medium-oxidized nanoadsorbents [**PhosO(1:8)**, **PhosO(1:4)**] display a strong affinity with OH^- anions, reaching adsorption energies of up to 3.1 eV that are high enough to remove any other less-stable adsorbate from the adsorption sites, including As(III) and As(V). Thus, arsenicals will be desorbed from medium-oxidized phosphorene by treatment with NaOH eluents, restoring the sorption sites for repetitive adsorption-desorption cycles. Note that OH^- anions can be further removed from nanoadsorbents by simple washing with deionized water until a neutral pH is achieved[13]. On the contrary, the recovery of highly oxidized phosphorene [**PhosO(1:2)**, **PhosO(1:1)**] with alkaline eluents does not appear like a feasible procedure, since the hydroxide uptake (E_{ads}<0.8 eV) do not overcome the sorption stability reached by arsenicals (E_{ads}>1.0 eV). This behavior emerges from the high oxygen content in **PhosO(1:2)** and **PhosO(1:1)**; this is negatively charged adsorption sites repel hydroxide anions with a larger magnitude than arsenicals due to the localized negative charge of OH^-.

Based on these results, medium-oxidized **PhosO(1:4)** nanoadsorbents (25% in oxygen content) show the optimal oxidizing degree for arsenic removal due to three main properties: i) higher adsorption strength for simultaneous As(III)/As(V) uptake compared to intrinsic phosphorene and **PhosO(1:8)** (13 % in oxygen content); ii) higher selectivity by As(III)/As(V) than H_2O molecules in aqueous solution, ensuring for low-pollutant mobility; and iii) straightforward recovery and reusability by a simple regeneration procedure via alkaline treatment (due to its strong selectivity by hydroxide anions at high pH). As a consideration, we choose the **PhosO(1:4)** nanoadsorbent as the best adsorbent candidate for further analyses in this work.

3.4. Adsorption mechanism

We attempt to provide a quantitative and readily physical interpretation of the adsorption mechanism by analyzing the specific role of physically intuitive meaningful terms with the ALMO-EDA method. EDA terms were organized as stabilizing (ΔE_{ELEC}, ΔE_{DISP}, ΔE_{CT}, ΔE_{POL}), and destabilizing terms (ΔE_{PAULI}, ΔE_{PREP}). Table 2 shows the EDA terms, and Fig. 3 displays the relative single percentage contributions (Φ_i, in %) of stabilizing EDA terms for a quick interpretation.

In the case of **As(III)–PhosO** complexes, electrostatic interactions (ΔE_{ELEC}) mainly govern the inner-sphere surface complexation, overcoming 58% of the total stabilizing energy. Then, permanent Coulombic electrostatic attraction is the main driving force determining the stability of **As(III)–PhosO** complexes in solution. In addition, we found stabilization gained by electrostatic interactions (ΔE_{ELEC}) enhances in up to two orders of magnitude upon adsorption on phosphorene oxide compared to the unoxidized material. For instance, the **As(III)–Phos** and **As(III)–PhosO** complexes are stabilized in $\Delta E_{ELEC} \approx -1.7$ and $\Delta E_{ELEC} \approx -3.5$ eV by electrostatic interactions, respectively (Table 2), corresponding to single stabilizing contributions of 58 and 60%, respectively (Fig. 3). Note also that the relative

Table 2. EDA terms. Energies are in eV; positive and negative values stand for repulsive (destabilizing) and attractive (stabilizing) interactions, respectively.

	stabilizing				Destabilizing	
system	ΔE_{ELEC}	ΔE_{POL}	ΔE_{CT}	ΔE_{DISP}	ΔE_{PAULI}	ΔE_{PREP}
As(III)–PhosO	3.48	0.41	1.16	0.95	5.21	0.31
As(V)$^{-}$–PhosO	6.50	6.48	4.77	1.03	13.07	2.32
As(V)$^{2-}$–PhosO	10.33	11.53	4.40	1.00	14.53	3.49
As(III)–Phos	2.07	0.15	0.44	0.80	2.56	0.08
As(V)$^{-}$–Phos	6.85	2.50	2.54	1.07	8.42	0.83
As(V)$^{2-}$–Phos	15.27	10.27	3.85	1.22	15.20	2.52

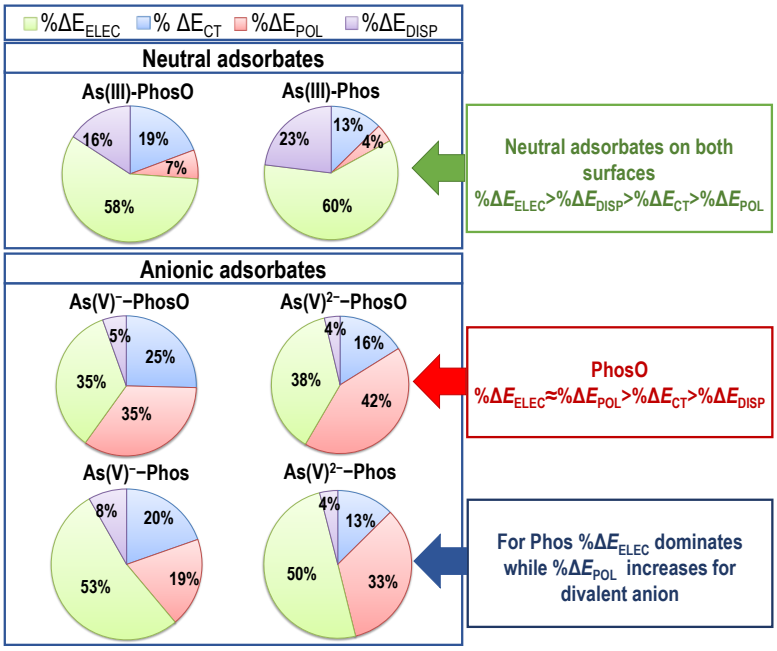

Fig. 3. Relative single percentage contributions (Φ_i, in %) of EDA terms.

single percentage contributions (Φ_i) are similar between pristine and oxidized adsorbents (Fig. 3), denoting that adsorption on both materials is governed by similar driving forces. In addition, the strong electrostatic contribution was documented in experimental studies of arsenic-phosphorene complexes due to the low adsorption heat in variable temperature experiments[25]. Electrostatic driving forces have also been described as the main stabilizing contribution for the adsorption stability of formaldehyde and heavy metals [e.g., Pb(II), Hg(II), and Cd(II)] onto phosphorene in the covalent and non-covalent regime[22,63].

On the other hand, charge-transfer and dispersion driving forces ($\Delta E_{CT}+\Delta E_{DISP}$) stand for up to 30% of the stability in the **As(III)–PhosO** complex, in agreement with a weak electron transfer (<~0.1|*e*|) in the As(III)→**PhosO** direction. In contrast, polarization stabilizing effects (ΔE_{POL}) are weak at the equilibrium distances, with contributions lower than 7% for neutral adsorbates because it is predominantly a short-range term.

EDA terms were also obtained for the **As(V)–PhosO** complexes to rationalize the differences between As(III) and As(V) adsorption. As(V) is mainly anionic in aqueous solution at pH=7; thus, electrostatics interactions will be directly proportional to the charge magnitude of anionic adsorbates and increasing as the As(V) negative charge increases. In fact, the ΔE_{ELEC} magnitude considerably increases for adsorbed As(V) species compared to the As(III) adsorption, denoting the key role of permanent electrostatic stabilization in the As(V) complexation as stated by Sharma and Sohn[49]. For instance, As(III), $As(V)^{-}$, and $As(V)^{2-}$ species are stabilized by electrostatic forces in ~3.5, 6.5, and 10.3 eV, respectively. Moreover, the stabilization gained by polarization effects (ΔE_{POL}) is almost equivalent to the stability gained through electrostatic forces ($\Delta E_{ELEC} \approx \Delta E_{POL}$), which are accounting for up to 82% of the total stabilizing energy (Fig. 3). Therefore, the inner-sphere surface complexation of As(V) species on phosphorene oxide is driven by the interplay of electrostatic and polarization effects. In this regard, when adsorbent and adsorbate approach, negatively charged As(V) cause a strong on-fragment relaxation of the **PhosO** nanoadsorbents due to As(V) nuclei/electrons and vice-versa; this relaxation occurs in the form of density rearrangements that create induced multipole moments favorably aligned (polarization), which increase the magnitude of electrostatic forces and, subsequently, the adsorption stability. Additionally, the charge-transfer stabilization (ΔE_{CT}) term shows a high contribution of up to 25% in the **As(V)–PhosO** complexes as a result of the high electron transfer (~0.6|*e*|) in the As(V)→**PhosO** direction, which is resulting of the polarizing phenomena as noted above. Additionally, dispersion effects play a minor role in the **As(V)–PhosO** complexes, standing for up to 5% of the total stabilizing energy.

306 Finally, destabilizing effects emerge at least ~80% due to Pauli repulsion (ΔE_{PAULI})
307 in all the cases because the geometrical structure of As(III)/As(V) is weakly influenced upon
308 adsorption. A high ΔE_{PAULI} term appears in the **As(V)–PhosO** complexes due to the strong
309 negative charge excesses in both the adsorbent and adsorbate (up to $\Delta E_{PAULI} \approx 14$ eV, Table
310 2). However, the magnitude of steric repulsion is lower than the main stabilizing forces
311 ($|\Delta E_{ELEC}+\Delta E_{POL}+\Delta E_{CT}|>\Delta E_{PAULI}$), leading to stable adsorption. Conversely, in the highly-
312 oxidized phosphorene nanoadsorbents [**PhosO(1:2)**, **PhosO(1:1)**], the arsenic uptake
313 comprises a large contribution of Pauli repulsion due to the high oxygen concentration on the
314 adsorbent surface. Consequently, Pauli repulsion is overcompensating all the attractive forces
315 ($|\Delta E_{ELEC}+\Delta E_{POL}+\Delta E_{CT}|<\Delta E_{PAULI}$), leading to the increase of the electron density kinetic
316 energy when negatively charged fragments are brought into close interaction[39,64]. The
317 latter explains why highly-oxidized phosphorene nanoadsorbents do not provide additional
318 adsorption performance for arsenic removal than medium-oxidized phosphorene.

319 An overview of the whole adsorption process along the dissociation path of the
320 **As(III)–PhosO** and **As(V)$^{-}$–PhosO** complexes as representative cases is presented (Fig. 4).
321 The dynamic adsorption process is determined in the first stages by the mass transport
322 between the **PhosO** nanoadsorbents and dissolved arsenicals in water (mass transfer step),
323 subsequently favored by the arsenic diffusion into the nanoadsorbent surface. In the
324 **As(III)–PhosO** complex, electrostatic and dispersion driving forces ($\Delta E_{ELEC}+\Delta E_{DISP} \approx \Delta E_{INT}$,
325 Fig. 4a) drive the mass transport at larger intermolecular distances (>4.4 Å). As a comparison,
326 the mass transport is only driven by dispersion forces on intrinsic phosphorene at larger
327 intermolecular distances (see the supporting material for details). The latter indicates
328 phosphorene oxidation favors the diffusion through the solvent media compared to intrinsic

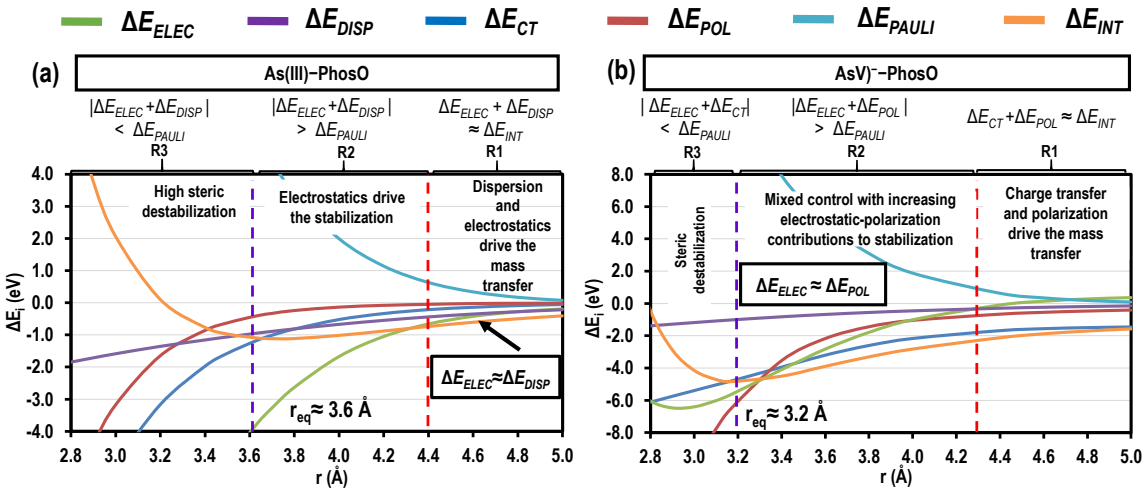

Fig. 4. EDA of **As(III)–PhosO** (**a**) and **As(V)⁻–PhosO** (**b**) complexes along its dissociation curve. The path is divided into three regions for analysis: R1, R2, and R3.

phosphorene because of long-range electrostatic effects at the early stages of the adsorption process, increasing the mass transfer and arsenic diffusion into the nanoadsorbent structure via charge-controlled interactions. Consequently, the time to reach the adsorption equilibrium is decreased. After the As(III) diffusion and until the intermolecular equilibrium distance is reached, the interplay between dispersion and electrostatic effects overcome the steric repulsion ($|\Delta E_{ELEC}+\Delta E_{DISP}|>\Delta E_{PAULI}$), leading to stable adsorption. Instead, the dissociation curve of **As(V)–PhosO** complexes shows that mass transport at larger intermolecular distances (>4.3 Å) is governed by long-range charge-transfer and polarizing effects as a result of the anionic charge of As(V) and the electrophilic character of **PhosO** ($\Delta E_{CT}+\Delta E_{POL}\approx\Delta E_{INT}$, Fig. 4b). Therefore, the time to reach the adsorption equilibrium is expected to be lesser for pentavalent arsenicals than trivalent ones. After the diffusion step, the **As(V)–PhosO** complexes are stabilized by a mixed and balanced contribution of short-range driving forces (e.g., electrostatics, charge-transfer, and polarization) until the equilibrium distance is reached, where ΔE_{POL} and ΔE_{ELEC} are dominant stabilizing effects and depending on the As(V) speciation.

3.5. Mobility and water-assisted adsorption

The adsorption stability in a water environment was examined to ensure low pollutant mobility after adsorption. A hybrid explicit-implicit solvation model was employed, where explicit H_2O molecules surround the adsorbate combined with the SMD solvation model to create the solvent reaction environment. In this way, the **As–PhosO** complexes were fully optimized to get insights into the adsorption stability under potential competition with H_2O molecules. It is noteworthy water molecules are weakly physisorbed onto intrinsic phosphorene [$E_{ads}(H_2O)$≈0.2 eV], forming H_2O clusters even at high pressures[28]. Therefore, the formation of water clusters around the adsorbed arsenicals could help the adsorption process, favoring the uptake stability.

We compare the **As–PhosO** complexes in an implicit and explicit solvation environment (Fig. 5). As can be seen, H_2O molecules form hydrogen-bonded clusters around the **As–PhosO** complexes, without pollutant desorption or pollutant decomposition in other

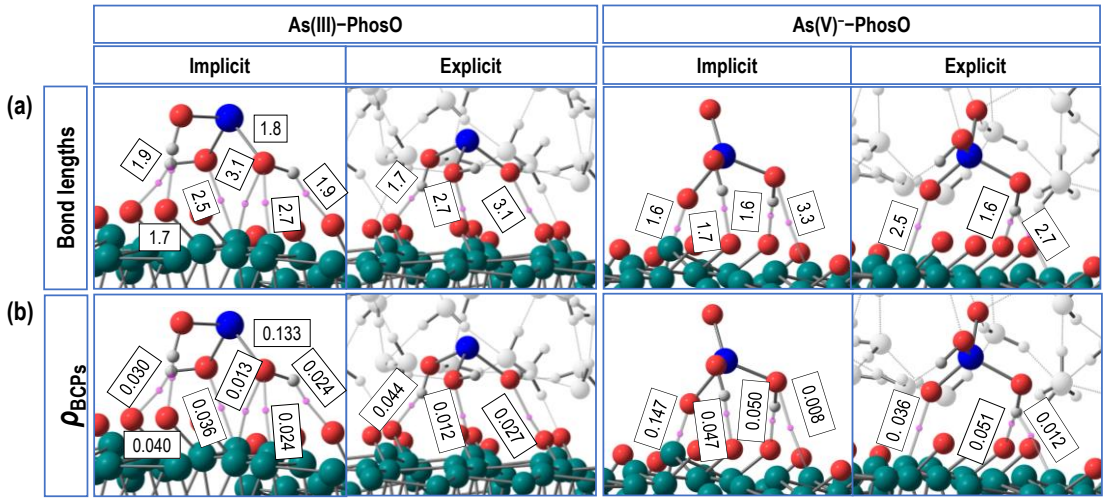

Fig. 5. Comparison between implicit (**non-assisted**) and explicitly (**water-assisted**) solvated arsenicals adsorbed onto **PhosO**. **a**) Intermolecular bond lengths (in Å) and **b**) electron densities at the bond critical points (ρ_i, in e/Bohr^3) are presented for comparison.

harmful compounds. These results indicate that **PhosO** nanoadsorbents allow avoiding the mobility phenomenon; even more, forming water clusters through hydrogen bonds could increase the stability of **As–PhosO** complexes. In other words, water molecules are not competitive factors for the simultaneous adsorption of As(III) and As(V) onto phosphorene oxide. Moreover, the water-assisted adsorption is dominated by hydrogen bonding formed by the acid hydrogens of arsenicals and the surface oxygen atoms of **PhosO**, showing bond lengths in the range of ~1.7–1.9 Å (Fig. 5a). Intermolecular O(As)···P(**PhosO**) interactions are also retained, while some hydroxyl groups of arsenicals are reoriented to form hydrogen bonds with H_2O molecules, but without desorption from the adsorbent surface.

Focusing on the nature of intermolecular interactions, the AIM analysis quantifies the electron density (ρ_i) at the intermolecular bond critical points [BCPs, points in space at which the first derivatives of the electron density vanish $\nabla\rho(r)=0$], which is quantitatively related the bonding strength. We note the intermolecular **As–PhosO** hydrogen bonding becomes stronger in an explicit water environment compared to the water-free modeling, characterized by ρ_i values at the BCPs in the range of 0.02–0.05 *e*/Bohr^3 (highly polarized closed-shell electrostatic interactions) (Fig. 5b). In the case of **As(V)–PhosO** complexes, the intermolecular O···P interactions display ρ_i values of up to 0.03 *e*/Bohr^3, indicating a weak coordinate and highly polarized covalent bonding (orbital interaction) between O and P atoms. This result is in agreement with the high contribution of charge-transfer and polarization stabilizing effects ($\Delta E_{CT}+\Delta E_{POL}$) into the stability of **As(V)$^-$–PhosO** complexes, which appear in orbital interactions. Therefore, the strong inner-sphere surface complexation exactly emerges from the interplay between strong intermolecular electrostatic interactions (hydrogen bonding) and/or highly polarized/coordinate covalent bonding from the chemical

viewpoint. Similar behavior has been described for arsenic adsorption onto metal-doped phosphorene in the chemisorption regime[50,51].

In summary, the strong adsorption stability and low arsenic mobility from the **As–PhosO** complexes can be explained based on three main properties: (i) low arsenic mobility is reached because water molecules forms clusters surrounding the adsorbate (water-assisted adsorption), favoring the intermolecular **As–PhosO** hydrogen bonding; (ii) **As(V)$^{-}$–PhosO** complexes are also stabilized by O···P weak coordinate bonding, which agrees with experimental results in phosphorene surfaces[24,25], increasing the charge-transfer and polarizing stabilizing effects as a result of orbital interactions. It is necessary to point out co-existing anionic species (such as Cl^{-}, CO_3^{2-}, PO_4^{3-}, and SO_4^{2-}) slightly suppress the arsenic adsorption capacity of oxidized layered materials[11,12,65]. Nevertheless, some co-existing species (e.g. citric acid) increases the arsenic adsorption efficiency of phosphorene, reaching a maximum adsorption capacity of 20 mg/g, respectively[25]. Suitable NCl amount (~0.1M) also increases the arsenic adsorption from ~40 to 95% by using graphene-oxide, without a larger competition for the adsorption sites with other co-existing anions (PO_4^{3-} and SO_4^{2-})[13]. Then, a suitable magnitude of ionic strength could be beneficial to improve the arsenic removal efficiency of layered oxides. In this regard, surface complexation modeling and vibrational spectroscopy experiments have established that ionic strength does not change the arsenic adsorption if arsenicals form inner-sphere surface complexes[66]; in opposition, outer-sphere surface complexes destabilizes at higher ionic strength values, decreasing the adsorption capacity. Therefore, phosphorene oxides are expected to retain their adsorption capacity/efficiency in the presence of co-existing anions due to the adsorption mechanism *via* inner-sphere surface complexation.

3.6. Adsorption free energies

We explored the adsorption process spontaneity in a temperature range of 300–1000 K (Fig. 6). At room temperature (300 K), the adsorption free energy (ΔG_{ads}) of the **As–PhosO** and **As–Phos** complexes is negative, denoting a spontaneous adsorption process. The temperature-dependent ΔG_{ads} profile shows the adsorption spontaneity decays as the temperature increases. In this regard, an exothermic reaction in water favors the spontaneous adsorption process (ΔH_{ads}<0), but entropic effects must oppose the reaction spontaneity (ΔS_{ads}<0), and it increases with the temperature until the reaction turns non-spontaneous, leading to desorption. Desorption temperatures of 369 and 635 K were found for **As(III)–Phos** and **As(III)–PhosO** complexes, insuring efficient adsorption in a wide temperature range; while desorption temperatures are out of range for pentavalent arsenicals. With this in mind, the surface regeneration could be assisted by thermal treatment in the selective adsorption of As(III) species.

Note that arsenic adsorption on solid surfaces can follow three different thermodynamic profiles: (i) an enthalpically governed reaction, where the adsorption

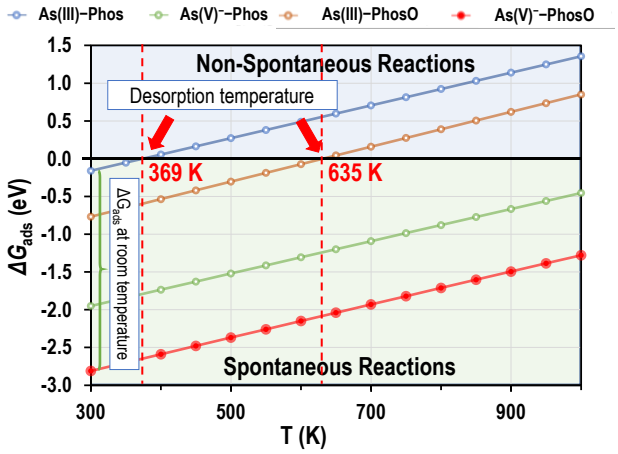

Fig. 6. ΔG_{ads} of arsenicals adsorption onto **Phos** and **PhosO** nanoadsorbents evaluated at temperatures T=300–1000 K, 1 atm.

418 spontaneity decays as the temperature increases; (ii) an entropically governed reaction, where
419 the adsorption spontaneity increases at higher temperatures; (iii) an enthalpic-entropically
420 governed reaction, where the adsorption spontaneity is favored in a broad temperature range.
421 In our case, the **As–Phos** and **As–PhosO** complexes show an enthalpic governed reaction,
422 which has also been described for the gaseous As_2O_3 adsorption onto carbonaceous
423 surfaces[67]. Ferric oxide-chitosan composites also show enthalpic governed adsorption
424 reactions with arsenicals, with desorption temperatures of 300−330 K[68]. Therefore, the
425 feature of enthalpically governed adsorption reactions can be exploited to regenerate the
426 material by thermal treatment and/or supporting other recovery treatments. In contrast, ferric
427 hydroxide and zirconium-based metal-organic framework are adsorbents with entropically
428 and enthalpic-entropically governed adsorption reactions, respectively[69,70].

429 **4. Conclusions**

430 We have theoretically elucidated the sorption properties of phosphorene oxide
431 nanoadsorbents for the simultaneous removal of inorganic As(III) and As(V) pollutants from
432 water. We found that phosphorene oxide forms stable inner-sphere surface complexes with
433 arsenicals even under aqueous environments, and it shows a strong affinity with highly
434 mobile As(III). Electrostatic driving forces govern the adsorption of neutral arsenicals, while
435 the interplay between electrostatic and polarization phenomena drives the uptake of anionic
436 arsenicals. Furthermore, the optimum adsorption efficiency is reached with a 25% in the
437 content of oxidizing groups, which also turns the phosphorene oxide nanoadsorbents
438 convenient to be recycled via simple alkaline treatment. Moreover, adsorption-free energies
439 show that the adsorption process is allowed in a wide range of ambient temperatures.

Acknowledgments

D.C-A and K.W-A acknowledge the financial support of CONICYT/FONDECYT projects N°11170289 and N°3200270. Computational resources were supported by SCC-PIDi-UTEM (CONICYT - FONDEQUIP - EQM180180). Powered@NLHPC: This research was partially supported by the supercomputing infrastructure of the NLHPC (ECM-02).

References

[1] K.R. Henke, Arsenic: Environmental chemistry, health threats and waste treatment, Wiley Online Library, 2009.

[2] J.R. Lloyd, E.T. Gnanaprakasam, N. Bassil, B.E. van Dongen, L.A. Richards, D.A. Polya, B.J. Mailloux, B.C. Bostick, A. van Geen, Environmental Arsenic in a Changing World, CRC Press, 2019. https://doi.org/10.1201/9781351046633.

[3] M.F. Hughes, Arsenic toxicity and potential mechanisms of action, Toxicol. Lett. 133 (2002) 1–16. https://doi.org/10.1016/S0378-4274(02)00084-X.

[4] S. Hirano, The accumulation and toxicity of methylated arsenicals in endothelial cells: important roles of thiol compounds, Toxicol. Appl. Pharmacol. 198 (2004) 458–467. https://doi.org/10.1016/j.taap.2003.10.023.

[5] S. Sharma, M.J. Bezbaruah, I. Ali, M. Choudhury, B. Bezbaruah, Theoretical Investigations on the π-π Stacking Interactions in Phenol-Water Complexes, Comput. Chem. 06 (2018) 15–25. https://doi.org/10.4236/cc.2018.62002.

[6] J. Chen, B.P. Rosen, The Arsenic Methylation Cycle: How Microbial Communities Adapted Methylarsenicals for Use as Weapons in the Continuing War for Dominance, Front. Environ. Sci. 8 (2020) 1–14. https://doi.org/10.3389/fenvs.2020.00043.

[7] P. Mondal, C.B. Majumder, B. Mohanty, Laboratory based approaches for arsenic remediation from contaminated water: Recent developments, J. Hazard. Mater. 137 (2006) 464–479. https://doi.org/10.1016/j.jhazmat.2006.02.023.

[8] D. Mohan, C.U. Pittman, Arsenic removal from water/wastewater using adsorbents—A critical review, J. Hazard. Mater. 142 (2007) 1–53. https://doi.org/10.1016/j.jhazmat.2007.01.006.

[9] A.S.K. Kumar, S.-J. Jiang, Chitosan-functionalized graphene oxide: A novel adsorbent an efficient adsorption of arsenic from aqueous solution, J. Environ. Chem. Eng. 4 (2016) 1698–1713. https://doi.org/10.1016/j.jece.2016.02.035.

[10] X. Luo, C. Wang, L. Wang, F. Deng, S. Luo, X. Tu, C. Au, Nanocomposites of graphene oxide-hydrated zirconium oxide for simultaneous removal of As(III) and As(V) from water, Chem. Eng. J. 220 (2013) 98–106. https://doi.org/10.1016/j.cej.2013.01.017.

[11] L. Yu, Y. Ma, C.N. Ong, J. Xie, Y. Liu, Rapid adsorption removal of arsenate by hydrous cerium oxide–graphene composite, RSC Adv. 5 (2015) 64983–64990. https://doi.org/10.1039/C5RA08922K.

[12] H. Su, Z. Ye, N. Hmidi, High-performance iron oxide–graphene oxide

nanocomposite adsorbents for arsenic removal, Colloids Surfaces A Physicochem. Eng. Asp. 522 (2017) 161–172. https://doi.org/10.1016/j.colsurfa.2017.02.065.
[13] L.-K. Wu, H. Wu, H.-B. Zhang, H.-Z. Cao, G.-Y. Hou, Y.-P. Tang, G.-Q. Zheng, Graphene oxide/CuFe2O4 foam as an efficient absorbent for arsenic removal from water, Chem. Eng. J. 334 (2018) 1808–1819. https://doi.org/10.1016/j.cej.2017.11.096.
[14] A.C. Reynosa-Martínez, G.N. Tovar, W.R. Gallegos, H. Rodríguez-Meléndez, R. Torres-Cadena, G. Mondragón-Solórzano, J. Barroso-Flores, M.A. Alvarez-Lemus, V.G. Montalvo, E. López-Honorato, Effect of the degree of oxidation of graphene oxide on As(III) adsorption, J. Hazard. Mater. 384 (2020) 121440. https://doi.org/10.1016/j.jhazmat.2019.121440.
[15] D. Cortés-Arriagada, A. Toro-Labbé, Improving As(<scp>iii</scp>) adsorption on graphene based surfaces: impact of chemical doping, Phys. Chem. Chem. Phys. 17 (2015) 12056–12064. https://doi.org/10.1039/C5CP01313E.
[16] R. Babar, M. Kabir, Transition Metal and Vacancy Defect Complexes in Phosphorene: A Spintronic Perspective, J. Phys. Chem. C. 120 (2016) 14991–15000. https://doi.org/10.1021/acs.jpcc.6b05069.
[17] J. Dai, X.C. Zeng, Bilayer Phosphorene: Effect of Stacking Order on Bandgap and Its Potential Applications in Thin-Film Solar Cells, J. Phys. Chem. Lett. 5 (2014) 1289–1293. https://doi.org/10.1021/jz500409m.
[18] P.D. Ye, Phosphorene as a new 2D material for device applications, in: 2015 73rd Annu. Device Res. Conf., IEEE, 2015: pp. 241–241. https://doi.org/10.1109/DRC.2015.7175657.
[19] A. Carvalho, M. Wang, X. Zhu, A.S. Rodin, H. Su, A.H. Castro Neto, Phosphorene: From theory to applications, Nat. Rev. Mater. 1 (2016). https://doi.org/10.1038/natrevmats.2016.61.
[20] P. Srivastava, K.P.S.S. Hembram, H. Mizuseki, K.R. Lee, S.S. Han, S. Kim, Tuning the electronic and magnetic properties of phosphorene by vacancies and adatoms, J. Phys. Chem. C. 119 (2015) 6530–6538. https://doi.org/10.1021/jp5110938.
[21] K. Cho, J. Yang, Y. Lu, Phosphorene: An emerging 2D material, J. Mater. Res. 32 (2017) 2839–2847. https://doi.org/10.1557/jmr.2017.71.
[22] S. Gazzari, D. Cortés-Arriagada, Uptake of formaldehyde onto doped phosphorene nanosheets: A cluster DFT study of single and co-adsorption states, J. Alloys Compd. 831 (2020) 154885. https://doi.org/10.1016/j.jallcom.2020.154885.
[23] Z. Mao, S. Dong, J. Li, X. Lin, X. Jian, P. Wu, Applied biaxial strain induced tunable sensing performance of green phosphorene monolayer towards small molecules: A DFT study, Appl. Surf. Sci. 536 (2021) 147759. https://doi.org/10.1016/j.apsusc.2020.147759.
[24] O.-P. Chen, Y.-J. Lin, W.-Z. Cao, C.-T. Chang, Arsenic removal with phosphorene and adsorption in solution, Mater. Lett. 190 (2017) 280–282. https://doi.org/10.1016/j.matlet.2017.01.030.
[25] Y.-J. Lin, W.-Z. Cao, T. Ou Yang, C.-H. Feng, C.-T. Chang, Deciphering the effect of citric acid on arsenic adsorption with phosphorene in aqueous solution, Sustain. Environ. Res. 29 (2019) 22. https://doi.org/10.1186/s42834-019-0021-8.
[26] B. Tian, B. Tian, B. Smith, M.C. Scott, Q. Lei, R. Hua, Y. Tian, Y. Liu, Facile bottom-up synthesis of partially oxidized black phosphorus nanosheets as metal-free photocatalyst for hydrogen evolution, Proc. Natl. Acad. Sci. 115 (2018) 4345–4350.

https://doi.org/10.1073/pnas.1800069115.
[27] J.M. Marmolejo-Tejada, A. Jaramillo-Botero, Partially-oxidized phosphorene sensor for the detection of sub-nano molar concentrations of nitric oxide: a first-principles study, Phys. Chem. Chem. Phys. 21 (2019) 19083–19091. https://doi.org/10.1039/C9CP03912K.
[28] G. Wang, W.J. Slough, R. Pandey, S.P. Karna, Degradation of phosphorene in air: understanding at atomic level, 2D Mater. 3 (2016) 025011. https://doi.org/10.1088/2053-1583/3/2/025011.
[29] G. Wang, R. Pandey, S.P. Karna, Phosphorene oxide: stability and electronic properties of a novel two-dimensional material, Nanoscale. 7 (2015) 524–531. https://doi.org/10.1039/C4NR05384B.
[30] A. Ziletti, A. Carvalho, P.E. Trevisanutto, D.K. Campbell, D.F. Coker, A.H. Castro Neto, Phosphorene oxides: Bandgap engineering of phosphorene by oxidation, Phys. Rev. B. 91 (2015) 085407. https://doi.org/10.1103/PhysRevB.91.085407.
[31] O.I. Malyi, K. V. Sopiha, C. Draxl, C. Persson, Stability and electronic properties of phosphorene oxides: from 0-dimensional to amorphous 2-dimensional structures, Nanoscale. 9 (2017) 2428–2435. https://doi.org/10.1039/C6NR08810D.
[32] W. Zhang, H. Enriquez, Y. Tong, A. Bendounan, A. Kara, A.P. Seitsonen, A.J. Mayne, G. Dujardin, H. Oughaddou, Epitaxial Synthesis of Blue Phosphorene, Small. 14 (2018) 1804066. https://doi.org/10.1002/smll.201804066.
[33] J.P. Perdew, K. Burke, M. Ernzerhof, Generalized gradient approximation made simple, Phys. Rev. Lett. 77 (1996) 3865–3868. https://doi.org/10.1103/PhysRevLett.77.3865.
[34] F. Neese, Software update: the ORCA program system, version 4.0, Wiley Interdiscip. Rev. Comput. Mol. Sci. 8 (2018) 4–9. https://doi.org/10.1002/wcms.1327.
[35] F. Weigend, Accurate Coulomb-fitting basis sets for H to Rn, Phys. Chem. Chem. Phys. 8 (2006) 1057. https://doi.org/10.1039/b515623h.
[36] S. Grimme, S. Ehrlich, L. Goerigk, Effect of the damping function in dispersion corrected density functional theory, J. Comput. Chem. 32 (2011) 1456–1465. https://doi.org/10.1002/jcc.21759.
[37] A. V. Marenich, C.J. Cramer, D.G. Truhlar, Universal solvation model based on solute electron density and on a continuum model of the solvent defined by the bulk dielectric constant and atomic surface tensions, J. Phys. Chem. B. 113 (2009) 6378–6396. https://doi.org/10.1021/jp810292n.
[38] S.F. Boys, F. Bernardi, The calculation of small molecular interactions by the differences of separate total energies. Some procedures with reduced errors, Mol. Phys. 19 (1970) 553–566. https://doi.org/10.1080/00268977000101561.
[39] P.R. Horn, Y. Mao, M. Head-Gordon, Probing non-covalent interactions with a second generation energy decomposition analysis using absolutely localized molecular orbitals, Phys. Chem. Chem. Phys. 18 (2016) 23067–23079. https://doi.org/10.1039/C6CP03784D.
[40] D.S. Levine, M. Head-Gordon, Energy decomposition analysis of single bonds within Kohn–Sham density functional theory, Proc. Natl. Acad. Sci. 114 (2017) 12649–12656. https://doi.org/10.1073/pnas.1715763114.
[41] P. Geerlings, F. De Proft, W. Langenaeker, Conceptual Density Functional Theory, Chem. Rev. 103 (2003) 1793–1874. https://doi.org/10.1021/cr990029p.

[42] P.C.F.M.P.R.J. Boyd, C.F. Matta, R.J. Boyd, A. Becke, The Quantum Theory of Atoms in Molecules, Wiley, Wiley-VCH, 2007. https://doi.org/10.1002/9783527610709.
[43] T. Lu, F. Chen, Multiwfn: A multifunctional wavefunction analyzer, J. Comput. Chem. 33 (2012) 580–592. https://doi.org/10.1002/jcc.22885.
[44] N. Saikia, M. Seel, R. Pandey, Stability and Electronic Properties of 2D Nanomaterials Conjugated with Pyrazinamide Chemotherapeutic: A First-Principles Cluster Study, J. Phys. Chem. C. 120 (2016) 20323–20332. https://doi.org/10.1021/acs.jpcc.6b06000.
[45] M.Y. Bakir, H.D. Ozaydin, T. Gorkan, O.Ü. Aktürk, G. Gökoğlu, E. Aktürk, S. Ciraci, Free-standing and supported phosphorene nanoflakes: Shape- and size-dependent properties, Appl. Surf. Sci. 506 (2020) 144756. https://doi.org/10.1016/j.apsusc.2019.144756.
[46] M. Ghashghaee, Z. Azizi, M. Ghambarian, Substitutional doping of black phosphorene with boron, nitrogen, and arsenic for sulfur trioxide detection: a theoretical perspective, J. Sulfur Chem. 41 (2020) 399–420. https://doi.org/10.1080/17415993.2020.1752692.
[47] R.G. Parr, P.K. Chattaraj, Principle of Maximum Hardness, J. Am. Chem. Soc. 113 (1991) 1854–1855. https://doi.org/10.1021/ja00005a072.
[48] A.L. Allred, E.G. Rochow, A scale of electronegativity based on electrostatic force, J. Inorg. Nucl. Chem. 5 (1958) 264–268. https://doi.org/10.1016/0022-1902(58)80003-2.
[49] V.K. Sharma, M. Sohn, Aquatic arsenic: Toxicity, speciation, transformations, and remediation, Environ. Int. 35 (2009) 743–759. https://doi.org/10.1016/j.envint.2009.01.005.
[50] D.E. Ortega, D. Cortés-Arriagada, Exploring the Nature of Interaction and Stability between Water-Soluble Arsenic Pollutants and Metal–Phosphorene Hybrids: A Density Functional Theory Study, J. Phys. Chem. A. 124 (2020) 3662–3671. https://doi.org/10.1021/acs.jpca.0c00532.
[51] D. Cortés-Arriagada, D.E. Ortega, Removal of arsenic from water using iron-doped phosphorene nanoadsorbents: A theoretical DFT study with solvent effects, J. Mol. Liq. 307 (2020) 112958. https://doi.org/10.1016/j.molliq.2020.112958.
[52] D. Cortés-Arriagada, A. Toro-Labbé, Improving As(III) adsorption on graphene based surfaces: Impact of chemical doping, Phys. Chem. Chem. Phys. 17 (2015) 12056–12064. https://doi.org/10.1039/c5cp01313e.
[53] A.F. Oliveira, A.C.Q. Ladeira, V.S.T. Ciminelli, T. Heine, H.A. Duarte, Structural model of arsenic(III) adsorbed on gibbsite based on DFT calculations, J. Mol. Struct. THEOCHEM. 762 (2006) 17–23. https://doi.org/10.1016/j.theochem.2005.08.038.
[54] A.C.Q. Ladeira, V.S.T. Ciminelli, H.A. Duarte, M.C.M. Alves, A.Y. Ramos, Mechanism of anion retention from EXAFS and density functional calculations: arsenic (V) adsorbed on gibbsite, Geochim. Cosmochim. Acta. 65 (2001) 1211–1217. https://doi.org/10.1016/S0016-7037(00)00581-0.
[55] Z. Wei, K. Liang, Y. Wu, Y. Zou, J. Zuo, D.C. Arriagada, Z. Pan, G. Hu, The effect of pH on the adsorption of arsenic(III) and arsenic(V) at the TiO 2 anatase [1 0 1] surface, J. Colloid Interface Sci. 462 (2016) 252–259. https://doi.org/10.1016/j.jcis.2015.10.018.
[56] D.M. Sherman, S.R. Randall, Surface complexation of arsenic(V) to iron(III)

(hydr)oxides: structural mechanism from ab initio molecular geometries and EXAFS spectroscopy, Geochim. Cosmochim. Acta. 67 (2003) 4223–4230. https://doi.org/10.1016/S0016-7037(03)00237-0.
[57] D. Cortés-Arriagada, A. Toro-Labbé, A theoretical investigation of the removal of methylated arsenic pollutants with silicon doped graphene, RSC Adv. 6 (2016) 28500–28511. https://doi.org/10.1039/C6RA03813A.
[58] M. Sen, A. Manna, P. Pal, Removal of arsenic from contaminated groundwater by membrane-integrated hybrid treatment system, J. Memb. Sci. 354 (2010) 108–113. https://doi.org/10.1016/j.memsci.2010.02.063.
[59] M. Habuda-Stanić, M. Nujić, Ž. Romić, A. Lončarić, M. Ergović Ravančić, E. Kralj, Arsenic preoxidation and its removal from groundwater using iron coagulants, Desalin. Water Treat. 56 (2015) 2105–2113. https://doi.org/10.1080/19443994.2014.959064.
[60] H. Elcik, S.O. Celik, M. Cakmakci, B. Özkaya, Performance of nanofiltration and reverse osmosis membranes for arsenic removal from drinking water, Desalin. Water Treat. 57 (2016) 20422–20429. https://doi.org/10.1080/19443994.2015.1111812.
[61] X. Song, L. Zhou, Y. Zhang, P. Chen, Z. Yang, A novel cactus-like Fe3O4/Halloysite nanocomposite for arsenite and arsenate removal from water, J. Clean. Prod. 224 (2019) 573–582. https://doi.org/10.1016/j.jclepro.2019.03.230.
[62] J.W. Brockgreitens, F. Heidari, A. Abbas, Versatile Process for the Preparation of Nanocomposite Sorbents: Phosphorus and Arsenic Removal, Environ. Sci. Technol. 54 (2020) 9034–9043. https://doi.org/10.1021/acs.est.9b07944.
[63] M. Ghashghaee, M. Ghambarian, Adsorption of toxic mercury, lead, cadmium, and arsenic ions on black phosphorous nanosheet: first-principles calculations, Struct. Chem. 30 (2019) 85–96. https://doi.org/10.1007/s11224-018-1173-6.
[64] P.R. Horn, Y. Mao, M. Head-Gordon, Defining the contributions of permanent electrostatics, Pauli repulsion, and dispersion in density functional theory calculations of intermolecular interaction energies, J. Chem. Phys. 144 (2016) 114107. https://doi.org/10.1063/1.4942921.
[65] M.-L. Chen, Y. Sun, C.-B. Huo, C. Liu, J.-H. Wang, Akaganeite decorated graphene oxide composite for arsenic adsorption/removal and its proconcentration at ultra-trace level, Chemosphere. 130 (2015) 52–58. https://doi.org/10.1016/j.chemosphere.2015.02.046.
[66] S. Goldberg, C.T. Johnston, Mechanisms of Arsenic Adsorption on Amorphous Oxides Evaluated Using Macroscopic Measurements, Vibrational Spectroscopy, and Surface Complexation Modeling, J. Colloid Interface Sci. 234 (2001) 204–216. https://doi.org/10.1006/jcis.2000.7295.
[67] Z. Gao, M. Zhao, G. Yan, H. Huang, W. Yang, X. Ding, C. Wu, lan D. Gates, Identifying the active sites of carbonaceous surface for the adsorption of gaseous arsenic trioxide: A theoretical study, Chem. Eng. J. 402 (2020) 125800. https://doi.org/10.1016/j.cej.2020.125800.
[68] B. Liu, D. Wang, H. Li, Y. Xu, L. Zhang, As(III) removal from aqueous solution using α-Fe2O3 impregnated chitosan beads with As(III) as imprinted ions, Desalination. 272 (2011) 286–292. https://doi.org/10.1016/j.desal.2011.01.034.
[69] K. Banerjee, G.L. Amy, M. Prevost, S. Nour, M. Jekel, P.M. Gallagher, C.D. Blumenschein, Kinetic and thermodynamic aspects of adsorption of arsenic onto granular ferric hydroxide (GFH), Water Res. 42 (2008) 3371–3378.

https://doi.org/10.1016/j.watres.2008.04.019.
[70] Z.J. Lin, H.Q. Zheng, Y.N. Zeng, Y.L. Wang, J. Chen, G.J. Cao, J.F. Gu, B. Chen, Effective and selective adsorption of organoarsenic acids from water over a Zr-based metal-organic framework, Chem. Eng. J. 378 (2019) 122196. https://doi.org/10.1016/j.cej.2019.122196.